Modeling, Tuning, and Performance Comparison of Second-Order-Generalized-Integrator-based FLLs

Golestan, Saeed; Guerrero, Josep M.; Quintero, Juan Carlos Vasquez; Abusorrah, Abdullah M.; Al-Turki, Yusuf

Published in:
I E E E Transactions on Power Electronics

DOI (link to publication from Publisher):
10.1109/TPEL.2018.2808246

Publication date:
2018

Document Version
Accepted author manuscript, peer reviewed version

Modeling, Tuning, and Performance Comparison of Advanced Second-Order Generalized Integrator-Based FLLs

Saeed Golestan, *Senior Member, IEEE*, Josep M. Guerrero, *Fellow, IEEE*, Juan. C. Vasquez, *Senior Member, IEEE*, Abdullah M. Abusorrah, *Senior Member, IEEE*, and Yusuf Al-Turki, *Senior Member, IEEE*

***Abstract*—The second-order generalized integrator-based frequency-locked loop (briefly called the SOGI-FLL) is a well-known tool for filtering and synchronization purposes in the power and energy applications. The SOGI-FLL, nevertheless, has a limited ability in rejecting the grid voltage disturbances. To deal with this problem, two advanced SOGI-FLLs have been proposed recently. In the first one, a SOGI-based filter is included inside the standard SOGI-FLL control loop, and in the second one, a SOGI-based filter is employed as the prefiltering stage of the SOGI-FLL. The small-signal modeling, tuning procedure, and detailed performance comparison of these advanced SOGI-FLLs have not been carried out yet. The aim of this paper is to cover these issues.**

***Index Terms*—Filters, frequency estimation, frequency-locked loop (FLL), phase detection, second-order generalized integrator (SOGI), synchronization.**

I. Introduction

Frequency-locked loop (FLL) is a nonlinear closed-loop control system that can be used in a wide variety of applications such as the grid synchronization [1]–[12], flux estimation and sensorless control of motor drives [13], [14], estimating delays of sinusoidal signals [15], measuring electromechanical oscillations [16], etc. The core component in the implementation of most FLLs is a generalized integrator (GI) [17].

Roughly speaking, the GI is a double integrator structure that provides an infinite gain at its resonant frequency and behaves as the amplitude integrator of sinusoidal signals. The GI can be realized in different ways [2]–[4], [18]. In implementing the FLL-based synchronization techniques, which is focused on in this paper, the most popular way is known as the second-order generalized integrator (SOGI). The SOGI has been originally developed in [19].

Manuscript received July 29, 2017; revised December 13, 2017; accepted February 4, 2018.

S. Golestan, J. M. Guerrero, and J. C. Vasquez are with the Department of Energy Technology, Aalborg University, Aalborg DK-9220, Denmark (e-mail: sgd@et.aau.dk; joz@et.aau.dk; juq@et.aau.dk).

A. M. Abusorrah and Y. Al-Turki are with the Renewable Energy Research Group, King Abdulaziz University, Jeddah, Saudi Arabia, and also with the Department of Electrical and Computer Engineering, Faculty of Engineering, King Abdulaziz University, Jeddah, Saudi Arabia (e-mail: aabusorrah@kau.edu.sa; yaturki@yahoo.com).

Color versions of one or more of the figures in this paper are available online at http://ieeexplore.ieee.org.

Fig. 1(a) illustrates the block diagram of the standard SOGI-FLL [1]. The SOGI-FLL is a simple yet valuable tool because, in addition to providing filtered in-phase and quadrature-phase versions of its input, it can estimate the phase, frequency, and amplitude of this signal. The SOGI-FLL, nevertheless, has a limited filtering capability. In other words, in the presence of DC offset, harmonics, and inter-harmonics, the estimated quantities by the SOGI-FLL suffer from oscillatory ripples. It should be mentioned that the small-signal modeling of phase/frequency estimation dynamics of the SOGI-FLL has been presented in [20].

To enhance the SOGI-FLL disturbance rejection capability, some attempts have been made in recent years. In [21], adding a DC offset estimation loop to the SOGI-FLL is suggested. This loop makes the SOGI-FLL immune to the DC offset disturbance effect and enhances its capability to filter sub-harmonics; however, it has no positive effect on the harmonic rejection capability of the SOGI-FLL.

In [1], a parallel configuration of multiple SOGIs (MSOGI) tuned at low-order harmonic frequencies is proposed. These SOGIs operate in a cooperative manner and, in addition to extracting some low-order harmonics, make the SOGI-FLL immune to the disturbance effect of these harmonics. Nevertheless, the number of parallel SOGIs and, therefore, the harmonic rejection capability of the MSOGI-FLL cannot be enhanced too much as it results in a high computational burden. Besides, the MSOGI-FLL may not be able to effectively suppress inter-harmonics because of the variability of their frequencies.

In [11], a SOGI-FLL with prefilter (SOGI-FLL-WPF) is suggested. The block diagram of the SOGI-FLL-WPF can be observed in Fig. 1(b). The prefilter in this structure is a frequency-adaptive band-pass filter and, according to [11], enhances the speed/accuracy tradeoff of the standard SOGI-FLL.

In [7] and [12], a structural resemblance between a SOGI-based quadrature signal generator (SOGI-QSG)[1] and a first-order low-pass filter (LPF) is established. This similarity indicates that replacing the only integrator of a first-order LPF with a SOGI results in the SOGI-QSG. Based on this finding and to enhance the filtering capability of the standard SOGI-

[1]The structure shown in Fig. 1(a) without the FLL, phase estimation, and amplitude detection parts is called the SOGI-QSG.

This article has been accepted for publication in a future issue of this journal, but has not been fully edited. Content may change prior to final publication. Citation information: DOI 10.1109/TPEL.2018.2808246, IEEE Transactions on Power Electronics

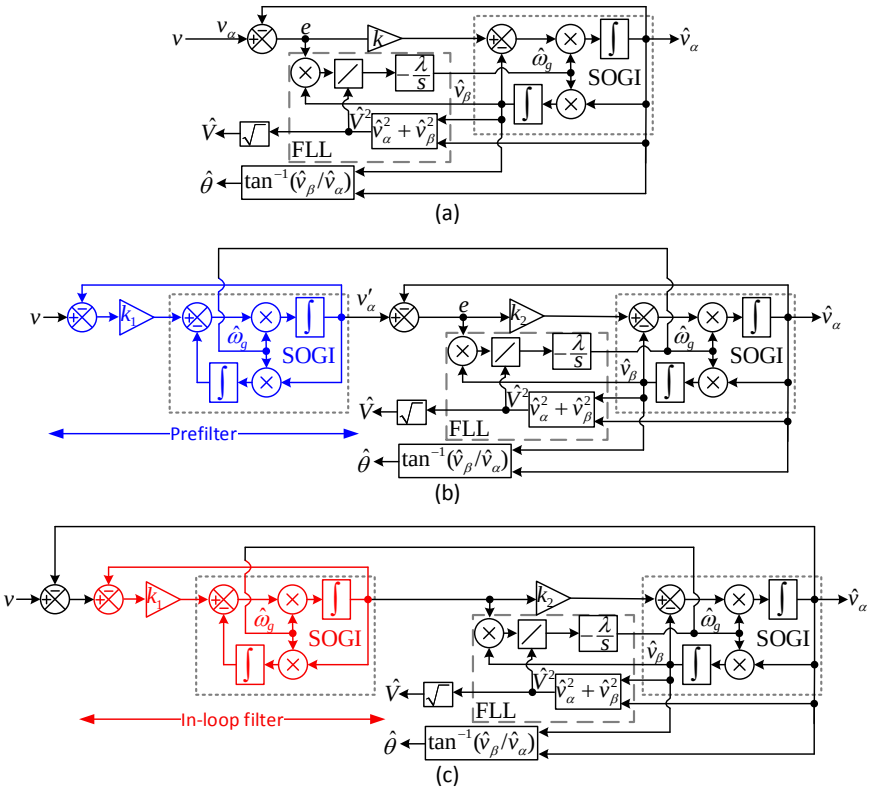

Fig. 1. (a) Standard SOGI-FLL, (b) SOGI-FLL with a SOGI-based prefilter (briefly referred to as the SOGI-FLL-WPF), and (c) SOGI-FLL with a SOGI-based in-loop filter (briefly referred to as the SOGI-FLL-WIF).

FLL, implementing a higher order SOGI-FLL by replacing two integrators of a second-order LPF with two SOGIs is suggested in [7] and [12]. A possible implementation of such SOGI-FLL, which is apparently different from that proposed in [12], can be observed in Fig. 1(c). This structure is called the SOGI-FLL with in-loop filter (SOGI-FLL-WIF). Notice that, depending on the implementation way of the second-order LPF, different structures may be achieved. All these structures are mathematically equivalent.

The small-signal modeling, analysis, and parameter tuning of these advanced SOGI-FLLs (i.e., SOGI-FLL-WPF and SOGI-FLL-WIF) have not yet been carried out. Besides, the real advantages and disadvantages of these advanced FLLs compared to each other and compared to the standard SOGI-FLL are unclear. The aim of this paper is to cover these issues.

II. Standard SOGI-FLL

Fig. 1(a), as mentioned before, illustrates the SOGI-FLL, which is a standard FLL in single-phase applications. By neglecting the FLL dynamics and assuming that $\hat{\omega}_g$ is a constant, the output signals of the SOGI, i.e., $\hat{v}_\alpha$ and $\hat{v}_\beta$, can be expressed in the s-domain as

$$\hat{v}_\alpha(s) = \underbrace{\frac{k\hat{\omega}_g s}{s^2 + k\hat{\omega}_g s + \hat{\omega}_g^2}}_{G_\alpha(s)} v(s) \tag{1}$$

$$\hat{v}_\beta(s) = \underbrace{\frac{k\hat{\omega}_g^2}{s^2 + k\hat{\omega}_g s + \hat{\omega}_g^2}}_{G_\beta(s)} v(s). \tag{2}$$

Fig. 2 shows the frequency response of the transfer functions $G_\alpha(s)$ and $G_\beta(s)$ for different values of k. As it can be seen, $G_\alpha(s)$ is a bandpass filter with a unity gain and a zero phase at the fundamental frequency. It means that the signal $\hat{v}_\alpha$ at the SOGI output is a filtered in-phase version of the single-phase grid voltage. The transfer function G_β, however, is an LPF (with the dc gain equal to k) which provides a unity gain and -90° phase at the fundamental frequency. It implies that the signal $\hat{v}_\beta$ is a filtered quadrature-phase version of the grid voltage.

Based on the above analysis and defining the grid voltage in the SOGI-FLL input as

$$v(t) = v_\alpha(t) = V\cos\underbrace{(\omega_g t + \varphi)}_{\theta} \tag{3}$$

where V, ω_g, φ, and θ are the grid voltage amplitude, angular frequency, initial phase angle, and phase angle, respectively, the signals $\hat{v}_\alpha$ and $\hat{v}_\beta$ at the SOGI output can be considered as

$$\hat{v}_\alpha(t) = \hat{V}\cos(\hat{\theta}) \tag{4}$$

$$\hat{v}_\beta(t) = \hat{V}\sin(\hat{\theta}). \tag{5}$$

In (4) and (5), $\hat{V}$ and $\hat{\theta}$ are the estimated amplitude and phase angle, respectively, and in the steady state are very close to (ideally equal to) V and θ, respectively. This is the basic assumption for the SOGI-FLL linearization, which is presented in the next section. Some parts of this linearization procedure has been already presented in [20], which are mentioned again

This article has been accepted for publication in a future issue of this journal, but has not been fully edited. Content may change prior to final publication. Citation information: DOI 10.1109/TPEL.2018.2808246, IEEE Transactions on Power Electronics

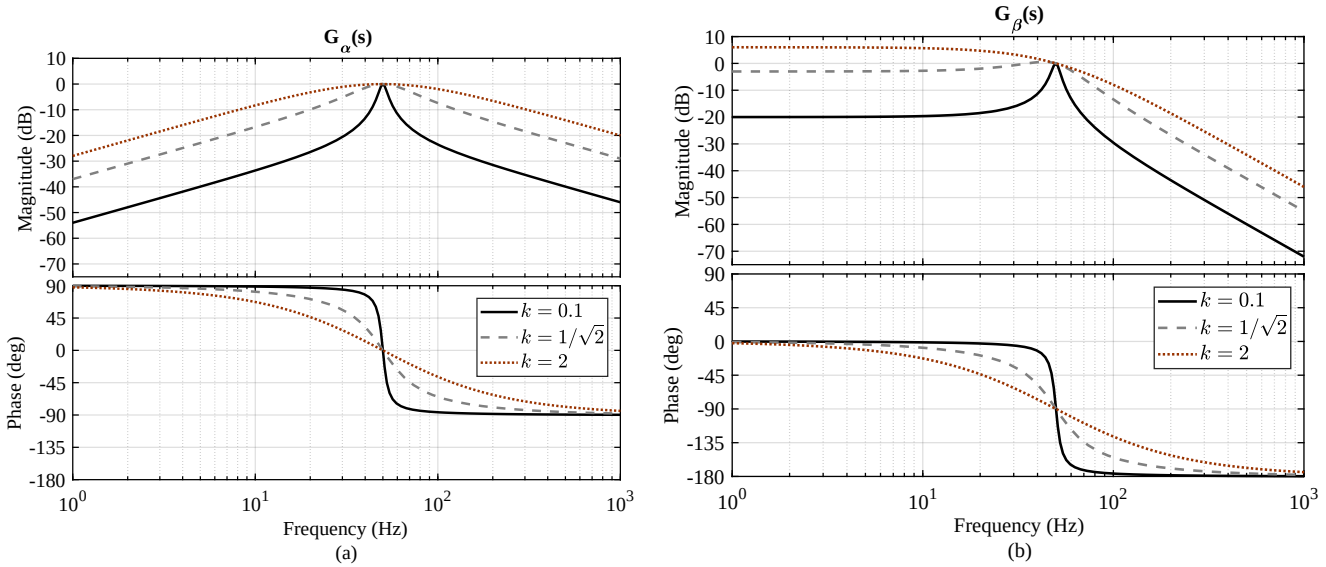

Fig. 2. Frequency response of (a) $G_\alpha(s)$ and (b) $G_\beta(s)$.

for the sake of completeness.

A. Linearization

From Fig. 1(a), the following differential equations, which describe the SOGI-FLL dynamics, can be obtained.

$$\dot{\hat{v}}_\alpha = \hat{\omega}_g \left[k\left(v_\alpha - \hat{v}_\alpha\right) - \hat{v}_\beta\right] \tag{6}$$

$$\dot{\hat{v}}_\beta = \hat{\omega}_g \hat{v}_\alpha \tag{7}$$

$$\dot{\hat{\omega}}_g = -\frac{\lambda}{\hat{V}^2}\left(v_\alpha - \hat{v}_\alpha\right)\hat{v}_\beta. \tag{8}$$

Substituting (3)-(5) into (8) results in

$$\begin{aligned}\dot{\hat{\omega}}_g &= -\frac{\lambda}{\hat{V}^2}\left[V\cos(\theta) - \hat{V}\cos(\hat{\theta})\right]\hat{V}\sin(\hat{\theta}) \\ &= \frac{\lambda}{2\hat{V}}\Big[\underbrace{V\sin(\theta-\hat{\theta})}_{\approx(\theta-\hat{\theta})} + \underbrace{\hat{V}\sin(2\hat{\theta}) - V\sin(\hat{\theta}+\theta)}_{\approx 0}\Big] \\ &\approx \frac{\lambda}{2}(\theta - \hat{\theta}).\end{aligned} \tag{9}$$

According to Fig. 1(a), the estimated phase angle by the SOGI-FLL can be expressed as

$$\hat{\theta} = \tan^{-1}(\hat{v}_\beta/\hat{v}_\alpha). \tag{10}$$

Differentiating (10) with respect to the time yields

$$\dot{\hat{\theta}} = \frac{\hat{v}_\alpha\dot{\hat{v}}_\beta - \dot{\hat{v}}_\alpha\hat{v}_\beta}{\hat{v}_\alpha^2 + \hat{v}_\beta^2} = \frac{\hat{v}_\alpha\dot{\hat{v}}_\beta - \dot{\hat{v}}_\alpha\hat{v}_\beta}{\hat{V}^2}. \tag{11}$$

Substituting (6) and (7) into (11) gives

$$\begin{aligned}\dot{\hat{\theta}} &= \frac{\overbrace{\left(\hat{v}_\alpha^2 + \hat{v}_\beta^2\right)}^{\hat{V}^2}\hat{\omega}_g - k\hat{\omega}_g\overbrace{\left(v_\alpha - \hat{v}_\alpha\right)\hat{v}_\beta}^{-\dot{\hat{\omega}}_g\hat{V}^2/\lambda}}{\hat{V}^2} \\ &= \hat{\omega}_g + \left(k\hat{\omega}_g/\lambda\right)\dot{\hat{\omega}}_g.\end{aligned} \tag{12}$$

Notice that the coefficient $\dot{\hat{\omega}}_g$, which is $k\hat{\omega}_g/\lambda$, is a time-variant term, because it depends on the estimated frequency $\hat{\omega}_g$. In this situation, the Laplace transform is not applicable. To deal with this problem, the estimated frequency in this coefficient is approximated by its nominal value as follows

$$\dot{\hat{\theta}} \approx \hat{\omega}_g + \left(k\omega_n/\lambda\right)\dot{\hat{\omega}}_g. \tag{13}$$

From Fig. 1(a), the estimated amplitude can be expressed as

$$\hat{V} = \sqrt{\hat{v}_\alpha^2 + \hat{v}_\beta^2}. \tag{14}$$

Differentiating (14) with respect to the time provides

$$\dot{\hat{V}} = \frac{\hat{v}_\alpha\dot{\hat{v}}_\alpha + \hat{v}_\beta\dot{\hat{v}}_\beta}{\sqrt{\hat{v}_\alpha^2 + \hat{v}_\beta^2}} = \frac{\hat{v}_\alpha\dot{\hat{v}}_\alpha + \hat{v}_\beta\dot{\hat{v}}_\beta}{\hat{V}}. \tag{15}$$

Substituting (6) and (7) into (15) yields

$$\dot{\hat{V}} = \frac{k\hat{\omega}_g\left(v_\alpha - \hat{v}_\alpha\right)\hat{v}_\alpha}{\hat{V}}. \tag{16}$$

Substituting (3) and (4) into (16) results in

$$\begin{aligned}\dot{\hat{V}} &= \frac{k\hat{\omega}_g\left[V\cos(\theta) - \hat{V}\cos(\hat{\theta})\right]\hat{V}\cos(\hat{\theta})}{\hat{V}} \\ &= \frac{k\hat{\omega}_g}{2}\Big(\overbrace{V\cos(\theta-\hat{\theta})}^{\approx 1} + \overbrace{V\cos(\theta+\hat{\theta}) - \hat{V}\cos(2\hat{\theta})}^{\approx 0} - \hat{V}\Big) \\ &\approx \frac{k\hat{\omega}_g}{2}\left(V - \hat{V}\right) \\ &\approx \frac{k\omega_n}{2}\left(V - \hat{V}\right).\end{aligned} \tag{17}$$

Notice that the estimated frequency $\hat{\omega}_g$ is again approximated by its nominal value.

Based on (9), (13), and (17), the linearized model depicted in Fig. 3 can be obtained for the SOGI-FLL. Using this model, the closed-loop transfer functions of the SOGI-FLL can be obtained as follows, which are very useful for the tuning procedure.

This article has been accepted for publication in a future issue of this journal, but has not been fully edited. Content may change prior to final publication. Citation information: DOI 10.1109/TPEL.2018.2808246, IEEE Transactions on Power Electronics

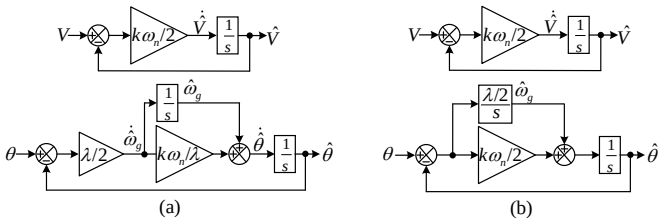

Fig. 3. (a) Linearized model of the SOGI-FLL, and (b) its alternative mathematically-equivalent representation.

$$\hat{V}(s) = \frac{k\omega_n/2}{s + k\omega_n/2} V(s) \tag{18}$$

$$\hat{\theta}(s) = \frac{(k\omega_n/2)\, s + \lambda/2}{s^2 + (k\omega_n/2)\, s + \lambda/2} \theta(s) \tag{19}$$

$$\hat{\omega}_g(s) = \frac{\lambda/2}{s^2 + (k\omega_n/2)\, s + \lambda/2} \omega_g(s). \tag{20}$$

Notice that $\omega_g(s) = s\theta(s)$.

B. Tuning Control Parameters

The characteristic polynomial of the transfer functions (19) and (20) is

$$s^2 + \underbrace{(k\omega_n/2)}_{2\zeta\omega_n'} s + \underbrace{\lambda/2}_{(\omega_n')^2} = 0 \tag{21}$$

where ζ and ω_n' are the damping factor and the natural frequency, respectively, and ω_n, as defined before, is the nominal value of the grid frequency. In most control texts, a damping factor equal to $1/\sqrt{2}$ is recommended because it results in an optimum tradeoff between the overshoot and settling time [22]. By considering $\zeta = 1/\sqrt{2}$ and using the definitions of ζ and ω_n' in (21), λ can be expressed as

$$\left.\begin{array}{l} \lambda = 2(\omega_n')^2 \\ \omega_n' = \frac{k\omega_n}{4\zeta} \end{array}\right\} \Rightarrow \lambda = \frac{k^2\omega_n^2}{8\zeta^2} = \frac{k^2\omega_n^2}{4}. \tag{22}$$

The equation (22) describes λ as a function of k. Therefore, both parameters of the SOGI-FLL are determined by selecting a proper value for the SOGI gain k.

Selecting a large value for k (which corresponds to a larger value for λ) makes the SOGI-FLL dynamic response fast. It, nevertheless, results in a low disturbance rejection capability. It implies that the designer has to make a tradeoff decision. In this paper, $k = 1/\sqrt{2}$ is selected, which corresponds to $\lambda = 12337$. Notice that the SOGI-FLL is supposed to be a reference for comparison with the SOGI-FLL-WPF and SOGI-FLL-WIP and, as it will be shown in Section VI, the selected control parameters for the SOGI-FLL provides a fair condition of comparison.

III. SOGI-FLL-WPF

A. Linearization

Fig. 1(b), as mentioned before, illustrates the block diagram of the SOGI-FLL-WPF. The linearization of the SOGI-FLL-WPF can be carried out by following the same mathematical procedure as that described for the standard SOGI-FLL. Here, however, for the sake of simplicity and convenience, an intuitive approach is employed.

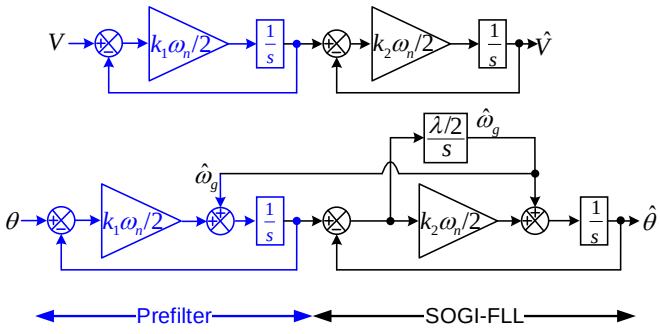

Fig. 4. Linearized model of the SOGI-FLL-WPF.

As shown in Fig. 1(b), the SOGI-FLL-WPF is the cascade connection of an adaptive prefilter and a SOGI-FLL. This prefilter is a SOGI-QSG, but only its α-axis output is used. The only difference of the prefilter compared to the SOGI-FLL is the lack of an FLL for adapting its center frequency. Notice that the prefilter uses the frequency feedback signal from the SOGI-FLL for adapting itself to the grid frequency variations. Therefore, the overall model of the SOGI-FLL-WPF can be obtained by cascading two SOGI-FLL models as shown in Fig. 4, in which the integrator modeling the FLL dynamics in the prefilter part is replaced by a frequency feedback from the SOGI-FLL part.

According to Fig. 4, the closed-loop transfer functions of the SOGI-FLL-WPF can be obtained as

$$\hat{V}(s) = \frac{(k_1\omega_n/2)\,(k_2\omega_n/2)}{(s + k_1\omega_n/2)\,(s + k_2\omega_n/2)} V(s) \tag{23}$$

$$\hat{\theta}(s) = \frac{\left[k_1k_2\omega_n^2/4\right] s + k_1\lambda\omega_n/4}{s^3 + \left[(k_1 + k_2)\,\omega_n/2\right] s^2 + \left[k_1k_2\omega_n^2/4\right] s + k_1\lambda\omega_n/4} \theta(s) \tag{24}$$

$$\hat{\omega}_g(s) = \frac{k_1\lambda\omega_n/4}{s^3 + \left[(k_1 + k_2)\,\omega_n/2\right] s^2 + \left[k_1k_2\omega_n^2/4\right] s + k_1\lambda\omega_n/4} \omega_g(s). \tag{25}$$

These transfer functions describe the dynamics of the SOGI-FLL-WPF and are very useful for the tuning procedure.

B. Tuning Control Parameters

The poles of the closed-loop transfer function (23) are both real. This corresponds to a damping factor equal to or greater than unity. A damping factor greater than unity makes the transient response of (23) (which describes the amplitude estimation dynamics) overdamped and, therefore, too slow. Consequently, a damping factor equal to unity is selected here, which corresponds to identical poles and, therefore, $k_1 = k_2$.

According to Fig. 1(b), the prefilter extracts the fundamental component of the grid voltage and feeds it to the SOGI-FLL. Assuming that $\hat{\omega}_g$ is a constant, the transfer function relating the extracted fundamental component by the prefilter to the grid voltage can be expressed as

$$v_\alpha'(s) = \frac{k_1\hat{\omega}_g s}{s^2 + k_1\hat{\omega}_g s + \hat{\omega}_g^2} v(s). \tag{26}$$

This article has been accepted for publication in a future issue of this journal, but has not been fully edited. Content may change prior to final publication. Citation information: DOI 10.1109/TPEL.2018.2808246, IEEE Transactions on Power Electronics

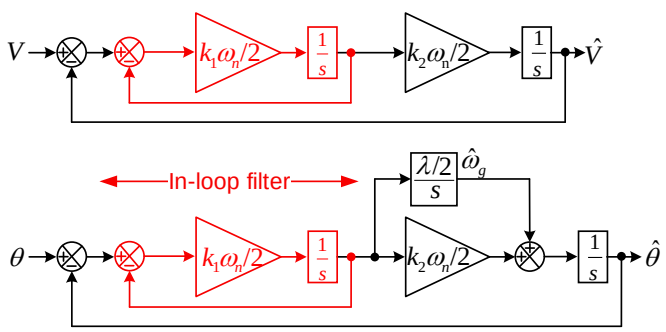

Fig. 5. Linearized model of the SOGI-FLL-WIF.

Based on (26), it can be concluded that $k_1 = \sqrt{2}$ is the best choice. Notice that this selection corresponds to a damping factor equal to $1/\sqrt{2}$ that ensure an optimum tradeoff between overshoot and settling time in the fundamental component extraction by the prefilter.

The characteristic polynomials of (24) and (25) are equal to

$$s^3 + \left[(k_1 + k_2)\,\omega_n/2\right] s^2 + \left[k_1 k_2 \omega_n^2/4\right] s + k_1\lambda\omega_n/4 = 0. \tag{27}$$

As (27) is a third-order polynomial, it must have at least one real pole. Therefore, it can be expressed as

$$\begin{aligned} s^3 + \left[(k_1 + k_2)\,\omega_n/2\right] s^2 + \left[k_1 k_2 \omega_n^2/4\right] s + k_1\lambda\omega_n/4 \\ = \left[s + \gamma\omega_n'\right]\left[s^2 + 2\zeta\omega_n' s + (\omega_n')^2\right] \end{aligned} \tag{28}$$

where ζ and ω_n' denotes the damping factor and natural frequency, respectively, and γ is a factor that determines the location of the real pole.

By equating coefficients of equal power in s in both sides of (28) and considering that $k_1 = k_2 = \sqrt{2}$, the FLL gain λ can be expressed as

$$\lambda = \frac{2\,(\zeta + 1)\,\omega_n^2}{(2\zeta + 1)^3}. \tag{29}$$

Again, by selecting the optimum damping factor $\zeta = 1/\sqrt{2}$, the FLL gain λ can be calculated as $\lambda = 23948$.

IV. SOGI-FLL-WIF

A. Linearization

The linearized model of the SOGI-FLL-WIF can be obtained by following the same mathematical procedure used for the SOGI-FLL modeling or based on the same intuitive approach used for the SOGI-FLL-WPF modeling. Fig. 5 shows the linearized model of the SOGI-FLL-WIF.

According to Fig. 5, the closed-loop transfer functions relating the estimated amplitude, frequency, and phase angle to the actual ones can be obtained as

$$\hat{V}(s) = \frac{k_1 k_2 \omega_n^2/4}{s^2 + \left[k_1\omega_n/2\right] s + k_1 k_2 \omega_n^2/4} V(s) \tag{30}$$

$$\hat{\theta}(s) = \frac{\left[k_1 k_2 \omega_n^2/4\right] s + k_1\lambda\omega_n/4}{s^3 + \left[k_1\omega_n/2\right] s^2 + \left[k_1 k_2 \omega_n^2/4\right] s + k_1\lambda\omega_n/4} \theta(s) \tag{31}$$

$$\hat{\omega}_g(s) = \frac{k_1\lambda\omega_n/4}{s^3 + \left[k_1\omega_n/2\right] s^2 + \left[k_1 k_2 \omega_n^2/4\right] s + k_1\lambda\omega_n/4} \omega_g(s). \tag{32}$$

These transfer functions are very helpful for tuning the control parameters and evaluating the FLL dynamics.

B. Tuning Control Parameters

According to Fig. 5, the open-loop transfer function relating the phase error to the estimated phase angle can be obtained as

$$\hat{\theta}(s) = \overbrace{\frac{\left(k_1 k_2 \omega_n^2/4\right)\left(s + \overbrace{\lambda/(k_2\omega_n)}^{\omega_z}\right)}{s^2\underbrace{(s + k_1\omega_n/2)}_{\omega_p}}}^{G_{ol}(s)} \left[\theta(s) - \hat{\theta}(s)\right]. \tag{33}$$

The symmetrical optimum method [23], [24] is then used for selecting the control parameters (see Appendix A). Applying this design method to (33) gives

$$\begin{aligned} k_1 &= 2b\omega_c/\omega_n \\ k_2 &= 2\omega_c/\omega_n \\ \lambda &= 2\omega_c^2/b \end{aligned} \tag{34}$$

where b determines the phase margin (PM) as expressed in (39) in the Appendix A, and ω_c is the gain crossover frequency. Therefore, all parameters of the SOGI-FLL-WIP are determined by selecting proper values for b and ω_c.

Using (34), the characteristic polynomial of the closed-loop transfer function (31) can be rewritten as

$$\begin{aligned} s^3 + \left[k_1\omega_n/2\right] s^2 + \left[k_1 k_2 \omega_n^2/4\right] s + k_1\lambda\omega_n/4 \\ = s^3 + b\omega_c s^2 + b\omega_c^2 s + \omega_c^3 \\ = (s + \omega_c)(s^2 + \underbrace{[b-1]}_{2\zeta}\omega_c s + \omega_c^2). \end{aligned} \tag{35}$$

It can be observed that b determines the damping factor of the closed-loop poles. Similar to the case of the SOGI-FLL-WPF, the optimum damping factor $\zeta = 1/\sqrt{2}$ is selected, which corresponds to $b = 1 + \sqrt{2}$ and, therefore, $PM = 45°$ [see (39) in Appendix A].

The selected control parameters for the SOGI-FLL-WPF are corresponding to a crossover frequency equal to $2\pi 18.8$ rad/s. To have a fair comparison, the same value is chosen as the crossover frequency of the SOGI-FLL-WIF.

Considering the selected values for b and ω_c, i.e., $b = 1+\sqrt{2}$ and $\omega_c = 2\pi 18.8$ rad/s, the SOGI-FLL-WIF control parameters can be calculated according to (34) as

$$\begin{aligned} k_1 &= 2b\omega_c/\omega_n = 1.815 \\ k_2 &= 2\omega_c/\omega_n = 0.752 \\ \lambda &= 2\omega_c^2/b = 11559. \end{aligned} \tag{36}$$

V. Model Accuracy Assessment

In Sections II, III, and IV, the small-signal modeling of the SOGI-FLL, SOGI-FLL-WPF, and SOGI-FLL-WIP were conducted. To ensure that the these models are reliable, their

This article has been accepted for publication in a future issue of this journal, but has not been fully edited. Content may change prior to final publication. Citation information: DOI 10.1109/TPEL.2018.2808246, IEEE Transactions on Power Electronics

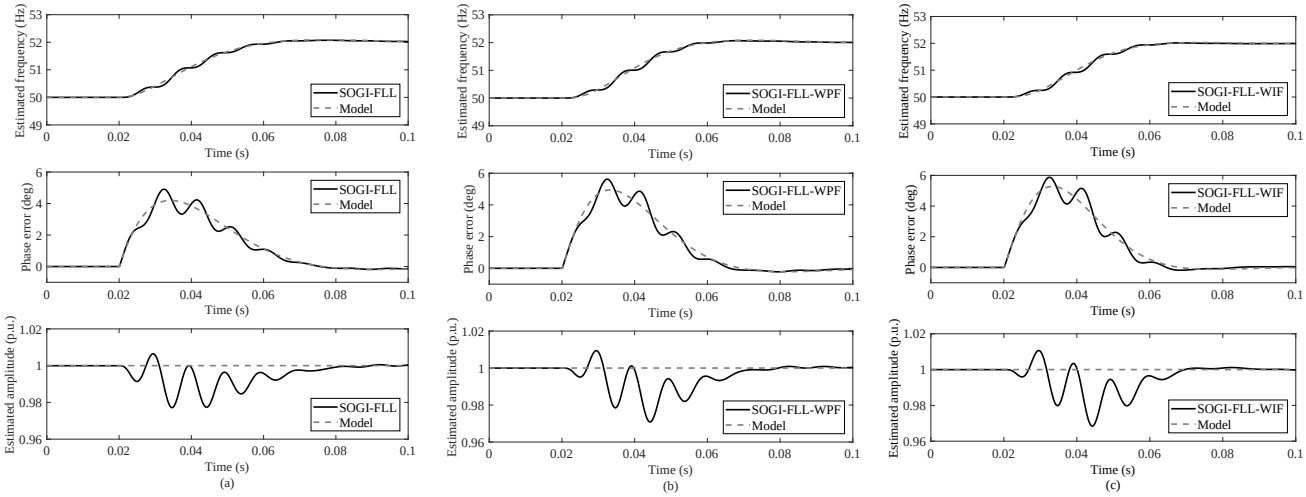

Fig. 6. Obtained results using (a) standard SOGI-FLL and its linearized model, (b) SOGI-FLL-WPF and its linearized model, and (c) SOGI-FLL-WIF and its linearized model in response to Test 1.

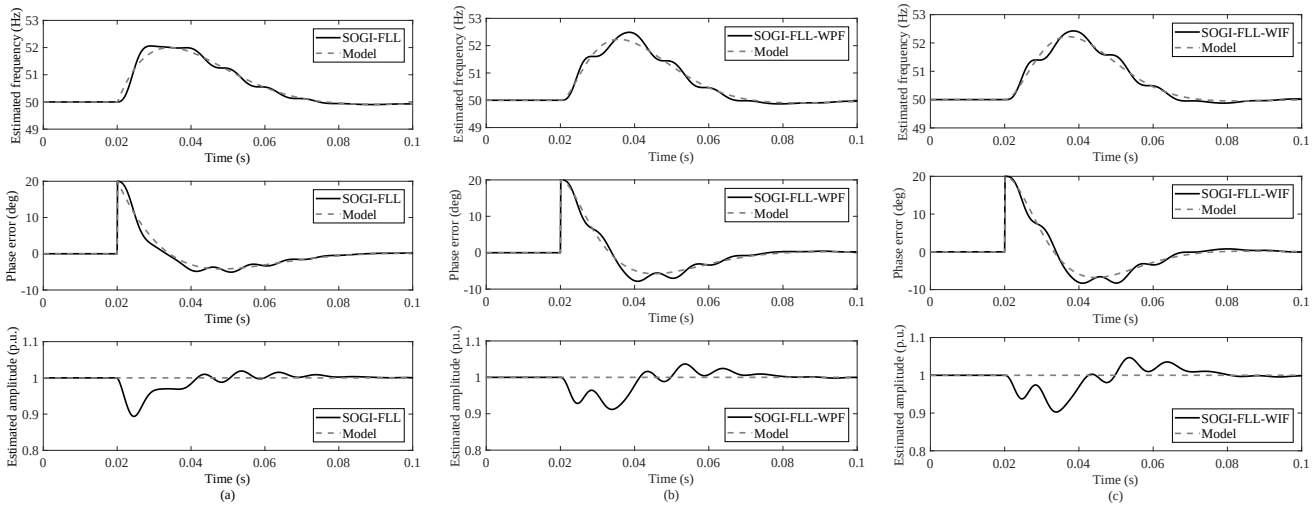

Fig. 7. Obtained results using (a) standard SOGI-FLL and its linearized model, (b) SOGI-FLL-WPF and its linearized model, and (c) SOGI-FLL-WIF and its linearized model in response to Test 2.

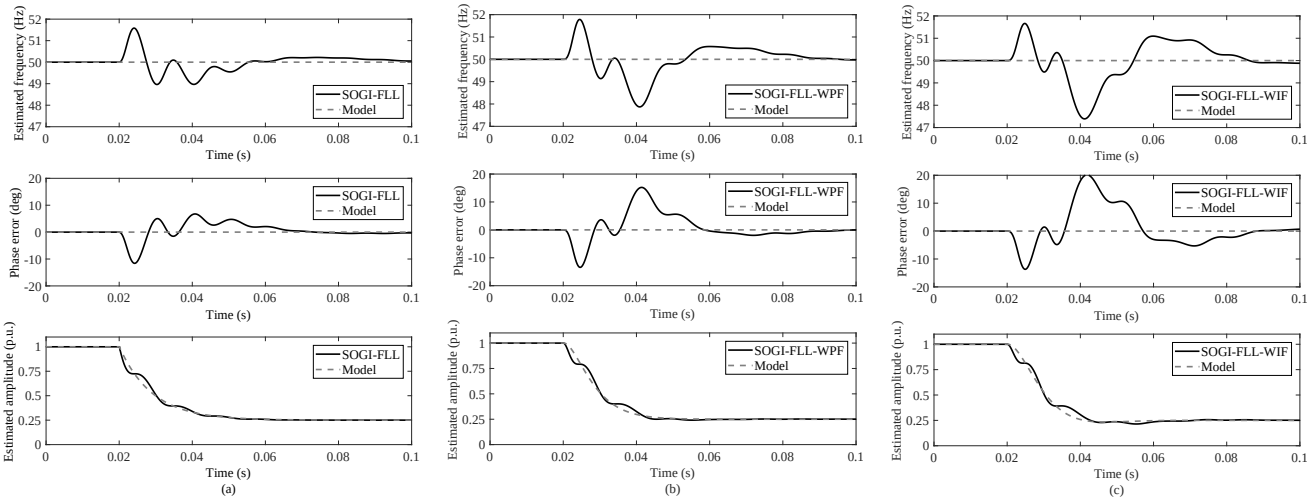

Fig. 8. Obtained results using (a) standard SOGI-FLL and its linearized model, (b) SOGI-FLL-WPF and its linearized model, and (c) SOGI-FLL-WIF and its linearized model in response to Test 3.

TABLE I
CONTROL PARAMETERS

FLL	Parameters
Standard SOGI-FLL	$k = 1/\sqrt{2}$, $\lambda = 12337$
SOGI-FLL-WPF	$k_1 = \sqrt{2}$, $k_2 = \sqrt{2}$, $\lambda = 23948$
SOGI-FLL-WIF	$k_1 = 1.815$, $k_2 = 0.752$, $\lambda = 11559$

accuracy should be evaluated. For this purpose, the following tests are conducted in the Matlab/Simulink environment and the results predicted by the linearized models are compared with those obtained by the FLLs under study.

- Test 1: The grid voltage experiences a $+2$ Hz frequency step change.
- Test 2: A $+20^\circ$ phase jump happens.
- Test 3: A 0.75 p.u. voltage sag occurs.

The sampling frequency throughout this study is 10 kHz.

Figs. 6-8 show the obtained results. It can be observed that the linearized models of all FLLs predict their average behaviors[2] with a good accuracy. These models, however, cannot predict the coupling between the estimated phase/frequency and amplitude. This is the main limitation of the linearized models.

VI. PERFORMANCE COMPARISON

In this section, the performance of the standard SOGI-FLL, SOGI-FLL-WPF, and SOGI-FLL-WIF are compared using some experimental results, which are obtained using the dSPACE 1006 platform. The grid voltage signal is generated using the dSPACE. The control parameters of all FLLs are summarized in Table I. In obtaining all experimental results, the sampling frequency is fixed at 10 kHz. The discretization of SOGIs is carried out using the third-order Adams-Bashforth method, in which an integrator is approximated by $\frac{T_s}{12}\frac{23z^{-1}-16z^{-2}+5z^{-3}}{1-z^{-1}}$ [25]. Some other approaches for the discretization of SOGIs can be found in [26], [27].

Five tests are considered:

- Test A: The frequency of the grid voltage suddenly changes from 50 Hz to 52 Hz.
- Test B: A 0.5 p.u. voltage sag with 60° phase jump happens. The grid frequency is at its nominal value.
- Test C: The grid voltage is harmonically distorted with low-order harmonics. The magnitude of harmonics are $V_3 \approx 0.054$ p.u., $V_5 \approx 0.048$ p.u., $V_7 \approx 0.022$ p.u., $V_9 \approx 0.005$ p.u., $V_{11} \approx 0.012$ p.u., $V_{13} \approx 0.006$ p.u. This corresponds to a total harmonic distortion (THD) around 7.7%. The grid frequency is fixed at its nominal value during this test.
- Test D: A large DC component (0.1 p.u.) is suddenly added to the grid voltage.
- Test E: The grid voltage contains a 1-Hz sub-harmonic with the magnitude of 0.1 p.u.

Figs. 9 and 10 show the performances of all FLLs in response to Tests A and B, respectively. It can be observed

[2]These models cannot predict the transient double-frequency oscillations in their corresponding FLLs because they have a linear time-invariant nature.

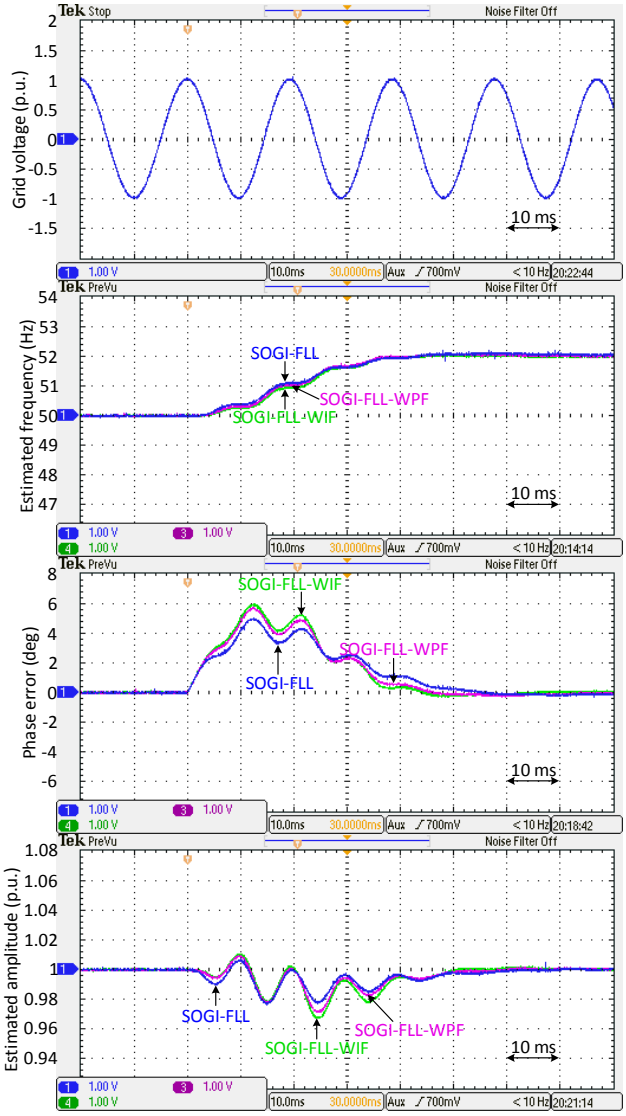

Fig. 9. Experimental results for Test A.

that all FLLs have a close speed of response (around 2.5 cycles of the nominal frequency) in estimating the grid voltage parameters. The only difference is that the quantities estimated by the SOGI-FLL experience rather smaller overshoots than those extracted by the SOGI-FLL-WPF and SOGI-FLL-WIF.

Fig. 11 illustrates the obtained results in response to Test C. The SOGI-FLL-WPF and SOGI-FLL-WIF demonstrate a close performance in this test and provide a bit higher harmonic filtering capability than the standard SOGI-FLL.

The obtained results in response to tests D and E can be observed in Figs. 12 and 13, respectively. As shown, the SOGI-FLL-WPF and SOGI-FLL-WIF, again, have a close performance and completely reject the DC component and effectively suppress the sub-harmonic. The standard SOGI-FLL, however, suffers from large oscillatory errors in the presence of these disturbances.

Fig. 14 illustrates open-loop Bode plots of the FLLs under study. These plots are obtained using open-loop transfer functions relating the phase error signal to the estimated phase

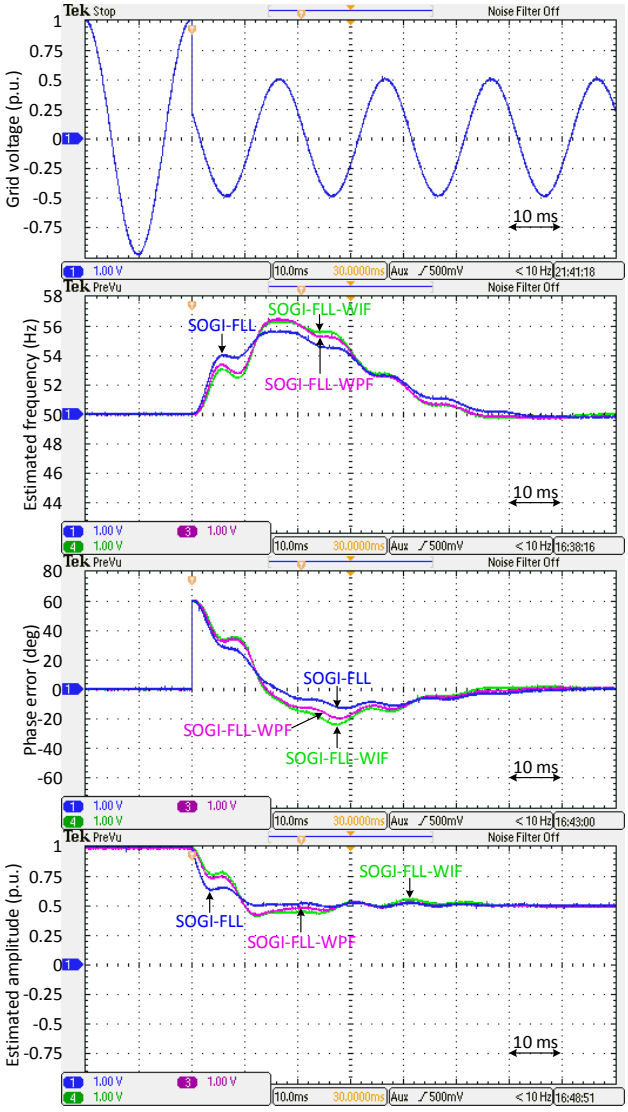

Fig. 10. Experimental results for Test B.

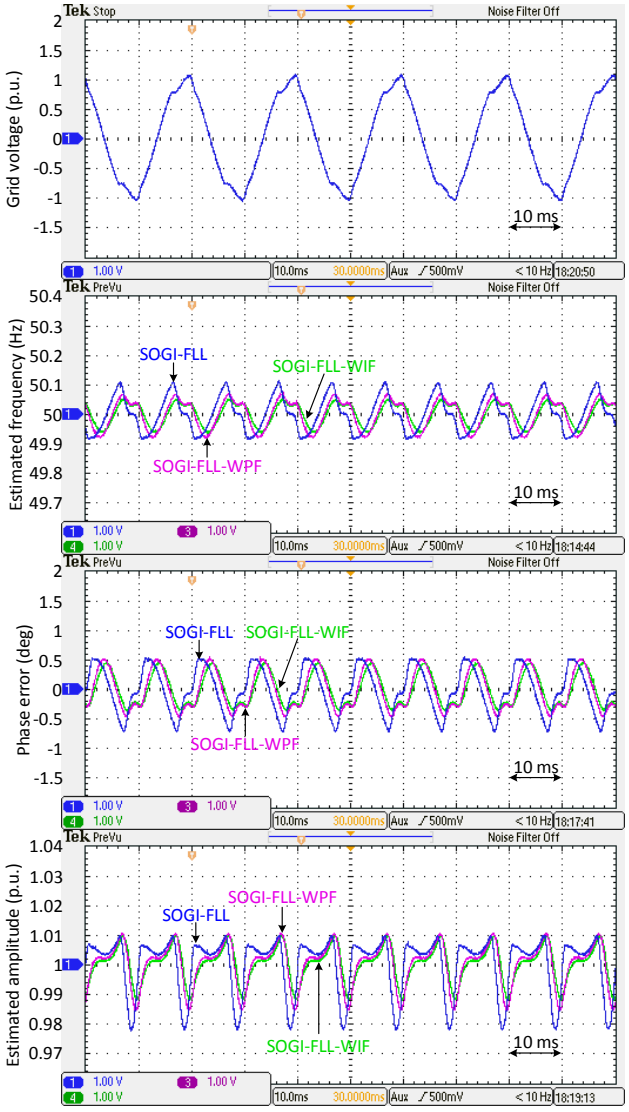

Fig. 11. Experimental results for Test C.

angle in the linearized model of the FLLs under study. Notice that the linearized model of the SOGI-FLL-WPF (Fig. 4) does not have a standard form. Therefore, to achieve the aforementioned open-loop transfer function, it should first be rearranged to its standard form by applying the block diagram algebra. Fig. 14 shows that all FLLs have a very close crossover frequency. It confirms the fair condition of comparison among them and explains their close speed of response during transients. It can also be observed that the SOGI-FLL has a higher PM than the SOGI-FLL-WPF and SOGI-FLL-WIF. That is the reason why in the Test B, the estimated quantities by the SOGI-FLL experience lower overshoots.

Table II compares the computational burden of all FLLs. This table indicates that the SOGI-FLL-WPF and SOGI-FLL-WIF demand a bit higher computational effort than the SOGI-FLL.

VII. Conclusion

In this paper, the small-signal modeling of the standard SOGI-FLL and two advanced SOGI-FLLs (SOGI-FLL-WPF and SOGI-FLL-WIF) were presented. Based on the derived models, systematic design approaches for selecting the control parameters of these FLLs were proposed. To ensure that the linearized models are accurate, a model accuracy assessment was conducted using some simulation studies. The obtained results demonstrate that the linearized models predict the average dynamic behavior of FLLs with a high accuracy. They, nevertheless, cannot predict the coupling between the amplitude and phase/frequency variables. Finally, using some experimental tests, a performance comparison among the standard SOGI-FLL, SOGI-FLL-WPF, and SOGI-FLL-WIF under a fair condition was conducted. The obtained results indicate that

- The SOGI-FLL-WPF and SOGI-FLL-WIF have a very close performance in all tests.
- The SOGI-FLL-WPF and SOGI-FLL-WIF, contrary to the standard SOGI-FLL which suffers from large os-

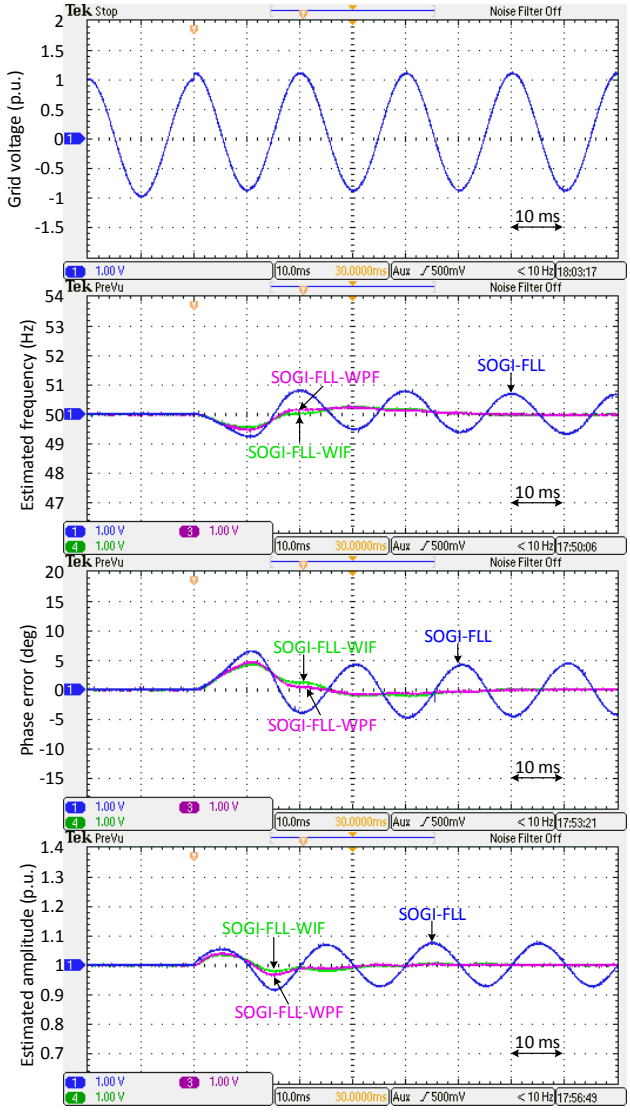

Fig. 12. Experimental results for Test D.

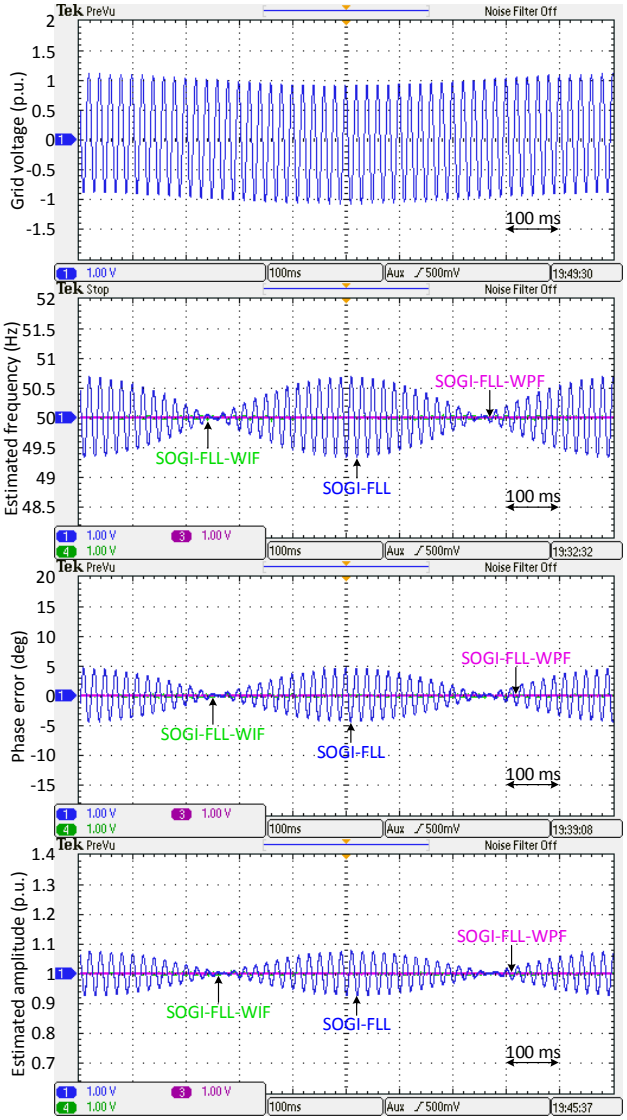

Fig. 13. Experimental results for Test E.

cillatory errors in the presence of DC offset and sub-harmonics, effectively reject these disturbances. Besides, they offer a bit higher capability in filtering the grid voltage harmonics.

- All FLLs have a close speed of response during transients. The estimated quantities by the SOGI-FLL, nevertheless, undergo a bit smaller overshoots.

It should be emphasized here that the above-mentioned advantages of the SOGI-FLL-WPF and SOGI-FLL-WIF come at the cost of a bit higher computational burden and a lower stability margin compared to the SOGI-FLL.

APPENDIX A
OVERVIEW OF SYMMETRICAL OPTIMUM METHOD

Assume that the open-loop transfer function of a closed-loop control system (with unity feedback) is as

$$G_{ol}(s) = \frac{\omega_p}{s+\omega_p}\frac{k_p s + k_i}{s^2} = \frac{\omega_p k_p (s + \overbrace{k_i/k_p}^{\omega_z})}{s^2(s+\omega_p)} \qquad (37)$$

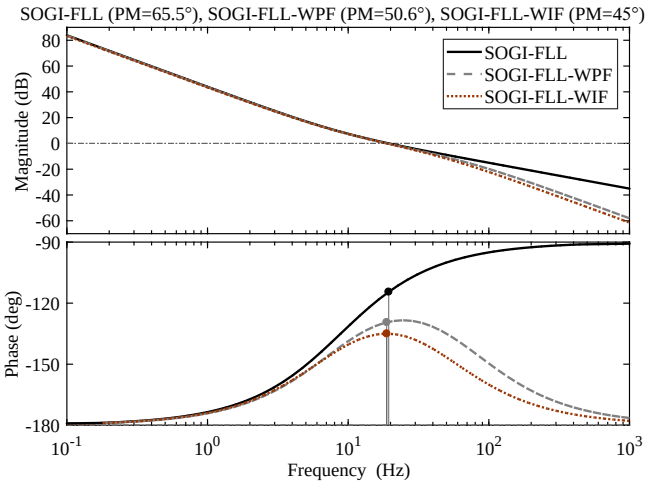

Fig. 14. Open-loop Bode plots.

where k_p, k_i, and ω_p are the control parameters. The open-loop pole ω_p is considered as $\omega_p = b^2\omega_z$, where b is a positive

TABLE II
NUMBER OF MATHEMATICAL OPERATIONS AND STATE VARIABLES (INTEGRATORS) IN THE IMPLEMENTATION OF THE SOGI-FLL, SOGI-FLL-WPF, AND SOGI-FLL-WIF. IT: INVERSE TANGENT, AND SQRT: SQUARE ROOT

	$\times$	$\div$	$\pm$	IT	SQRT	Integrators
SOGI-FLL	7	2	3	1	1	3
SOGI-FLL-WPF	10	2	5	1	1	5
SOGI-FLL-WIF	10	2	5	1	1	5

factor.

Using (37), the PM can be calculated as

$$PM = -\tan^{-1}(\omega_c/\omega_p) + \tan^{-1}(\omega_c/\omega_z) \tag{38}$$

where ω_c is the gain crossover frequency. The PM is maximized if $\omega_c = \sqrt{\omega_p \omega_z} = b\omega_z = \omega_p/b$ [23], [24]. Substituting this condition into (38) results in

$$PM = \tan^{-1}\left[\frac{b^2-1}{2b}\right]. \tag{39}$$

Using (37) and according to the definition of the crossover frequency (i.e., $|G_{ol}(j\omega_c)| = 1$) and the obtained condition for maximizing the PM, we have

$$1 = \frac{k_p \omega_p \sqrt{\omega_c^2+\omega_z^2}}{\omega_c^2\sqrt{\omega_c^2+\omega_p^2}} = \frac{k_p}{\omega_c} \quad \Rightarrow \quad k_p = \omega_c. \tag{40}$$

In summary, all control parameters can be expressed as

$$\begin{aligned} k_p &= \omega_c \\ k_i &= \omega_z k_p = \omega_c^2/b \\ \omega_p &= b\omega_c. \end{aligned} \tag{41}$$

ACKNOWLEDGMENT

This project was funded by the Deanship of Scientific Research (DSR), King Abdulaziz University, Jeddah, under grant no. (RG-6-135-38). The Authors, therefore, acknowledge with thanks DSR technical and financial support.

REFERENCES

[1] P. Rodriguez, A. Luna, I. Candela, R. Mujal, R. Teodorescu, and F. Blaabjerg, "Multiresonant frequency-locked loop for grid synchronization of power converters under distorted grid conditions," *IEEE Trans. Ind. Electron.*, vol. 58, no. 1, pp. 127–138, Jan. 2011.

[2] P. Rodriguez, A. Luna, R. S. Munoz-Aguilar, I. Etxeberria-Otadui, R. Teodorescu, and F. Blaabjerg, "A stationary reference frame grid synchronization system for three-phase grid-connected power converters under adverse grid conditions," *IEEE Trans. Power Electron.*, vol. 27, no. 1, pp. 99–112, Jan. 2012.

[3] D. Yazdani, M. Mojiri, A. Bakhshai, and G. Joos, "A fast and accurate synchronization technique for extraction of symmetrical components," *IEEE Trans. Power Electron.*, vol. 24, no. 3, pp. 674–684, Mar. 2009.

[4] M. Mojiri and A. R. Bakhshai, "An adaptive notch filter for frequency estimation of a periodic signal," *IEEE Trans. Autom. Control*, vol. 49, no. 2, pp. 314–318, Feb. 2004.

[5] J. Matas, M. Castilla, L. G. de Vicuna, J. Miret, E. Alarcon-Gallo, and A. Camacho, "Fast grid synchronization technique based on a multiple cascaded general integrator scheme for distributed generation inverters," in *2012 IEEE International Symposium on Industrial Electronics*, May. 2012, pp. 1003–1010.

[6] J. Matas, H. Martin, J. de la Hoz, A. Abusorrah, Y. A. Al-Turki, and M. Al-Hindawi, "A family of gradient descent grid frequency estimators for the SOGI filter," *IEEE Trans. Power Electron.*, vol. PP, no. 99, pp. 1–1, 2017.

[7] Z. Xin, X. Wang, Z. Qin, M. Lu, P. C. Loh, and F. Blaabjerg, "An improved second-order generalized integrator based quadrature signal generator," *IEEE Trans. Power Electron.*, vol. 31, no. 12, pp. 8068–8073, Dec. 2016.

[8] W. Li, X. Ruan, C. Bao, D. Pan, and X. Wang, "Grid synchronization systems of three-phase grid-connected power converters: A complex-vector-filter perspective," *IEEE Trans. Ind. Electron.*, vol. 61, no. 4, pp. 1855–1870, Apr. 2014.

[9] E. Oviedo, N. Vazquez, and R. Femat, "Synchronization technique of grid-connected power converters based on a limit cycle oscillator," *IEEE Trans. Ind. Electron.*, vol. 65, no. 1, pp. 709–717, Jan. 2018.

[10] H. Liu, Y. Xing, and H. Hu, "Enhanced frequency-locked loop with a comb filter under adverse grid conditions," *IEEE Trans. Power Electron.*, vol. 31, no. 12, pp. 8046–8051, Dec. 2016.

[11] J. Matas, M. Castilla, J. Miret, L. G. de Vicuna, and R. Guzman, "An adaptive prefiltering method to improve the speed/accuracy tradeoff of voltage sequence detection methods under adverse grid conditions," *IEEE Trans. Ind. Electron.*, vol. 61, no. 5, pp. 2139–2151, May. 2014.

[12] Z. Xin, R. Zhao, P. Mattavelli, P. C. Loh, and F. Blaabjerg, "Re-investigation of generalized integrator based filters from a first-order-system perspective," *IEEE Access*, vol. 4, pp. 7131–7144, 2016.

[13] Z. Xin, R. Zhao, F. Blaabjerg, L. Zhang, and P. C. Loh, "An improved flux observer for field-oriented control of induction motors based on dual second-order generalized integrator frequency-locked loop," *IEEE J. Emerging Sel. Top. Power Electron.*, vol. 5, no. 1, pp. 513–525, Mar. 2017.

[14] R. Zhao, Z. Xin, P. C. Loh, and F. Blaabjerg, "A novel flux estimator based on multiple second-order generalized integrators and frequency-locked loop for induction motor drives," *IEEE Trans. Power Electron.*, vol. 32, no. 8, pp. 6286–6296, Aug. 2017.

[15] M. Ghadiri-Modarres, M. Mojiri, and M. Karimi-Ghartemani, "New adaptive algorithm for delay estimation of sinusoidal signals with unknown frequency," *IEEE Trans. Instrum. Meas.*, vol. 64, no. 9, pp. 2360–2366, Sep. 2015.

[16] M. Mansouri, M. Mojiri, M. A. Ghadiri-Modarres, and M. Karimi-Ghartemani, "Estimation of electromechanical oscillations from phasor measurements using second-order generalized integrator," *IEEE Trans. Instrum. Meas.*, vol. 64, no. 4, pp. 943–950, Apr. 2015.

[17] X. Yuan, W. Merk, H. Stemmler, and J. Allmeling, "Stationary-frame generalized integrators for current control of active power filters with zero steady-state error for current harmonics of concern under unbalanced and distorted operating conditions," *IEEE Trans. Ind. Appl.*, vol. 38, no. 2, pp. 523–532, Mar. 2002.

[18] B. Burger and A. Engler, "Fast signal conditioning in single phase systems," in *Proc. of European Conference on Power Electronics and Applications*, 2001.

[19] U. Nuss, "Blindleistungskompensation mit selbstgeführten stromrichter und kapazitivem energiespeicher," *Ph.D. dissertation, Karlsruhe Institute of Technology, Germany*, 1989.

[20] S. Golestan, E. Ebrahimzadeh, J. M. Guerrero, and J. C. Vasquez, "An adaptive resonant regulator for single-phase grid-tied VSCs," *IEEE Trans. Power Electron.*, vol. 33, no. 3, pp. 1867–1873, Mar. 2018.

[21] M. Karimi-Ghartemani, S. A. Khajehoddin, P. K. Jain, A. Bakhshai, and M. Mojiri, "Addressing DC component in PLL and notch filter algorithms," *IEEE Trans. Power Electron.*, vol. 27, no. 1, pp. 78–86, Jan. 2012.

[22] K. Ogata and Y. Yang, "Modern control engineering," 1970.

[23] S. Golestan, M. Monfared, F. D. Freijedo, and J. M. Guerrero, "Design and tuning of a modified power-based PLL for single-phase grid-connected power conditioning systems," *IEEE Trans. Power Electron.*, vol. 27, no. 8, pp. 3639–3650, Aug. 2012.

[24] W. Leonhard, *Control of electrical drives*. Springer Science & Business Media, 2012.

[25] M. Ciobotaru, R. Teodorescu, and F. Blaabjerg, "A new single-phase PLL structure based on second order generalized integrator," in *2006 37th IEEE Power Electronics Specialists Conference*, Jun. 2006, pp. 1–6.

[26] F. J. Rodriguez, E. Bueno, M. Aredes, L. G. B. Rolim, F. A. S. Neves, and M. C. Cavalcanti, "Discrete-time implementation of second order generalized integrators for grid converters," in *2008 34th Annual Conference of IEEE Industrial Electronics*, Nov. 2008, pp. 176–181.

[27] M. J. Diaz, E. Bueno, R. Mateos, F. J. Rodriguez, and E. Monmasson, "FPGA implementation of harmonic detector based on second order generalized integrators," in *2008 34th Annual Conference of IEEE Industrial Electronics*, Nov. 2008, pp. 2453–2458.